agriculture

MDPI

Article

A Computational Tool for Three-Point Hitch Geometry Optimisation Based on Weight-Transfer Minimisation

Lianet Avello Fernández, Mirko Maraldi *, Michele Mattetti and Massimiliano Varani

Department of Agricultural and Food Sciences (DISTAL), University of Bologna, Viale G. Fanin 50, 40127 Bologna, Italy; lianet.avello2@unibo.it (L.A.F.); michele.mattetti@unibo.it (M.M.); massimiliano.varani@unibo.it (M.V.)

* Correspondence: mirko.maraldi@unibo.it

Abstract: The weight-transfer effect, consisting of the change in dynamic load distribution between the front and the rear tractor axles, is one of the most impairing phenomena for the performance, comfort, and safety of agricultural operations. Excessive weight transfer from the front to the rear tractor axle can occur during operation or manoeuvring of implements connected to the tractor through the three-point hitch (TPH). In this respect, an optimal design of the TPH can ensure better dynamic load distribution and ultimately improve operational performance, comfort, and safety. In this study, a computational tool (the *Optimiser*) for the determination of a TPH geometry which minimises the weight-transfer effect is developed. The Optimiser is based on a constrained minimisation algorithm. The objective function to be minimized is related to the tractor front-to-rear axle load transfer during a simulated reference manoeuvre performed with a reference implement on a reference soil. Simulations are based on a dynamic model of the tractor-TPH-implement aggregate. The geometry determined by the Optimiser complies with the ISO-730 Standard functional requirements and other design requirements. The interaction between the soil and the implement during the simulated reference manoeuvre was successfully validated against experimental data. The simulation results show that the adopted reference manoeuvre is effective in triggering the weight-transfer effect, with the front axle load exhibiting a peak-to-peak value of 27.1 kN during the manoeuvre. A benchmark test was conducted starting from the geometry of a commercially available TPH; the test showed that the Optimiser, after 36 iterations, was able to find an optimised TPH geometry which allows to reduce the weight-transfer effect by 14.9%.

Keywords: Optimiser; constrained minimisation; tractor-TPH-implement model; front axle load

check for updates

Citation: Avello Fernández, L.; Maraldi, M.; Mattetti, M.; Varani, M. A Computational Tool for Three-Point Hitch Geometry Optimisation Based on Weight-Transfer Minimisation. *Agriculture* **2022**, *12*, 460. https://doi.org/10.3390/agriculture12040460

Academic Editor: Jin He

Received: 25 February 2022
Accepted: 23 March 2022
Published: 25 March 2022

1. Introduction

Nowadays, the topics of operational performance, efficiency, comfort, and safety have become of utmost importance for the designers of agricultural machinery and for the market as well [1,2]. One of the most impairing phenomena in terms of comfort, safety, and performance during agricultural operations is the weight-transfer effect [3], consisting of the dynamic change in load distribution between the front and rear wheels of the tractor, occurring during tillage operations or implement manoeuvring.

The loads resulting from the interaction between the implement and the soil are transmitted to the tractor through a hitching system. Especially in the case of implements connected to the tractor through the three-point hitch (TPH), an optimal design can ensure better dynamic load distribution and, consequently, can offer advantages in terms of operational performance, comfort, and safety; improve tractor lateral stability and levelling of the implement; and help prevent fatigue damage [4,5]. Indeed, implement extraction from the soil during headland turns is the primary cause of fatigue damage during field operation since it induces a significant load change in tractor axles [6].

Considering the range of variation of the TPH geometrical dimensions and the requirements prescribed by the Standards [7,8], designers are faced with the task of defining

the TPH geometry in order to meet several kinematic, functional, structural, working, and economical requirements [9,10]. With the purpose of determining the optimal TPH geometry, Ambike and Schmiedeler [11] proposed the application of Geometric Constraint Programming for the determination of kinematic TPH configurations that satisfy the constraints imposed by the ASAE Standard S217.12 [7]. The design tool developed in their study also allows the user to graphically visualize the effects of the different parameters on the resulting design geometry through a CAD package software. Kumar et al. [12] developed a computer program that locates the virtual hitch point of the tractor with respect to the depth of operation. The program ultimately optimizes the TPH geometry by making the virtual hitch point lie on the line of pull. Prasanna Kumar [13] developed a Newton–Raphson-based algorithm capable of generating the trajectory of the lower, upper, and virtual hitch points. The algorithm also determines the geometric performance parameters of the TPH and its mechanical advantage, expressed in terms of the ratio of the output force to the input force of the mechanism. The algorithm was run on a group of 165 different TPHs collected from Nebraska tractor test reports and, albeit no objective functions were formally defined, optimal designs were selected based on the kinematic performance parameters and the maximum mechanical advantage of the TPH. In a similar fashion, Dhruw et al. [14] developed a design tool in which the mechanical advantage of the mechanism acted as the performance parameter of the TPH. The mechanical advantage of the TPH was not the only parameter of mechanical performance assumed for the optimization of the TPH geometry. Molari et al. [15] proposed a design methodology based on a constrained optimization technique where the objective function to be maximised was related to the TPH lifting performance, as defined by the OECD Code 2 [16]. Constraints to the optimisation were provided by the ISO-730 [8] Standard requirements.

Albeit having provided valuable results in terms of TPH geometry optimization, the previous studies have not accounted for the influence of the TPH geometry on the transmission of the implement loads to the tractor. Notably, Bauer at al. [17] developed a model to investigate the effect of the TPH setup on the load distribution between the tractor rear wheels during in-furrow ploughing; from their study, it was possible to conclude that the load difference between the in-furrow and the on-land wheels can be significantly reduced by adjusting the length of the TPH upper link. Their work highlighted the central role of the TPH in transmitting the loads acting on the implement to the tractor; however, their focus was on the TPH setup and not on optimising the TPH design in order to improve the overall dynamic behaviour of the tractor.

The aim of the present work is to fill this gap by developing a design tool for the determination of an optimised TPH geometry which minimises the weight-transfer effect, thus improving the dynamic performance of the tractor-implement system. The geometry optimisation tool, referred to as the *Optimiser*, is based on a constrained mimisation algorithm. The objective function to be minimized by the algorithm is related to the tractor front-to-rear axle load transfer during a simulated reference manoeuvre performed with a reference implement on a reference soil. Simulations are based on a dynamic model of the aggregate system constituted by the tractor, the TPH, and the implement. Constraints to the minimisation problem arise from the ISO-730 Standard functional requirements and other design requirements.

2. Materials and Methods

A model of an agricultural tractor equipped with a front axle suspension and bearing an implement mounted on the rear TPH (Figure 1) was developed to evaluate the influence of the TPH geometry on the weight-transfer effect. The model was kept as simple as possible in order to reduce computation time; nevertheless, all the features responsible for describing the weight transfer effect were included. The external loads due to the interaction between the implement and the soil were also modelled. The following assumptions were made:

- The tractor is modelled as a system constituted by the tractor chassis and the front axle;

- The tractor chassis, the rear axle, each TPH link, and the implement behave as rigid bodies;
- Friction at the TPH joints can be neglected;
- Front and rear wheels are massless, each modelled as a linear spring and a viscous damper set in parallel between the vehicle and the ground;
- The front axle suspension system is modelled as a linear spring in parallel with a viscous damper;
- The ground surface is assumed to be horizontal;
- The tractor performs the reference manoeuvre while moving forward on a straight line at constant speed.

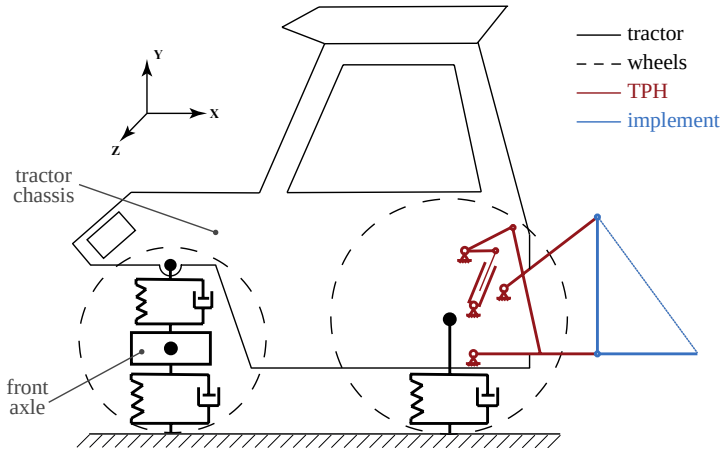

Figure 1. The tractor–TPH–implement model.

In order to reduce load transfer from the front to the rear tractor axle during implement operation or manoeuvring, a computational tool (the Optimiser) was developed, which optimises the TPH geometry while satisfying all the prescriptions of the ISO-730 Standard for TPH design. Scheme 1 depicts the structure of the Optimiser, whose kernel is constituted by a constrained minimisation algorithm. The inputs of the Optimiser are the parameters of the tractor equipped with the TPH subject to optimisation, the TPH category, and its initial geometry. The optimisation process is iterative, with the algorithm evaluating a trial TPH geometry (referred to as the current TPH geometry) at each step of the iteration. The evaluation is carried out through the tractor–TPH–implement model and consists of simulating a prescribed manoeuvre (referred to as the reference manoeuvre) performed with a reference implement while the tractor is running over a reference soil. The simulation allows to determine, for the current TPH geometry, the load on the tractor front axle as a function of time and, ultimately, to extract a measure of the weight transfer during the reference manoeuvre, which acts as the objective function associated with the current TPH geometry. The iterative optimisation process ends when a TPH geometry that minimises the objective function is found. Such optimised TPH geometry is the output of the Optimiser. The determination of the objective function follows the algorithm described in detail in Sections 2.1–2.5 and summarised in Scheme 2.

2.1. TPH Kinematic Analysis

Performing the kinematic analysis of the TPH is essential for simulating the reference manoeuvre and locating the position of the links where forces are exchanged between the implement and the TPH, and between the TPH and the tractor.

The kinematic analysis is performed in the median vertical–longitudinal plane (X–Y plane, Figure 2); the center of the rear axle is assumed as the origin of the reference frame. The mechanism is considered symmetrical about the X–Y plane and is divided into three subsystems: the triangle whose vertices are the points P_{hcp} , P_{hcd} , P_{cp} ; the quadrilateral whose vertices are the points P_{lap} , P_{lam} , P_{cd} , P_{cp}; and the quadrilateral whose vertices are

the points P_{lap} , P_{lad} , P_{uad} , P_{uap}. As proposed by Molari et al. [15], the analysis is based on the solution of a system of six nonlinear equations representing the condition of closure of the polygons which compose the three subsystems:

$$\begin{cases} X_{P_{hcp}} + l_{hc}\cos\varphi_{hc} - l_{chc}\cos(\varphi_c - \varphi_{chc}) - X_{P_{cp}} = 0 \\ Y_{P_{hcp}} + l_{hc}\sin\varphi_{hc} - l_{chc}\sin(\varphi_c - \varphi_{chc}) - Y_{P_{cp}} = 0 \\ X_{P_{cp}} + l_c\cos\varphi_c - l_{lr}\cos\varphi_{lr} - l_{lalr}\cos\varphi_{la} - X_{P_{lap}} = 0 \\ Y_{P_{cp}} + l_c\sin\varphi_c - l_{lr}\sin\varphi_{lr} - l_{lalr}\sin\varphi_{la} - Y_{P_{lap}} = 0 \\ X_{P_{uap}} + l_{ua}\cos\varphi_{ua} - m_h\cos\varphi_i - l_{la}\cos\varphi_{la} - X_{P_{lap}} = 0 \\ Y_{P_{uap}} + l_{ua}\sin\varphi_{ua} - m_h\sin\varphi_i - l_{la}\sin\varphi_{la} - Y_{P_{lap}} = 0 \end{cases} \quad (1)$$

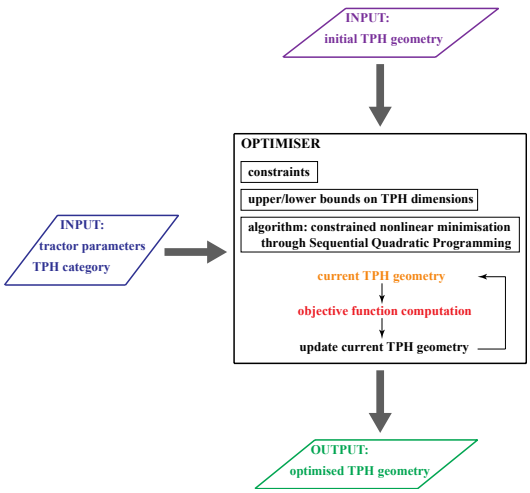

Scheme 1. Optimiser workflow.

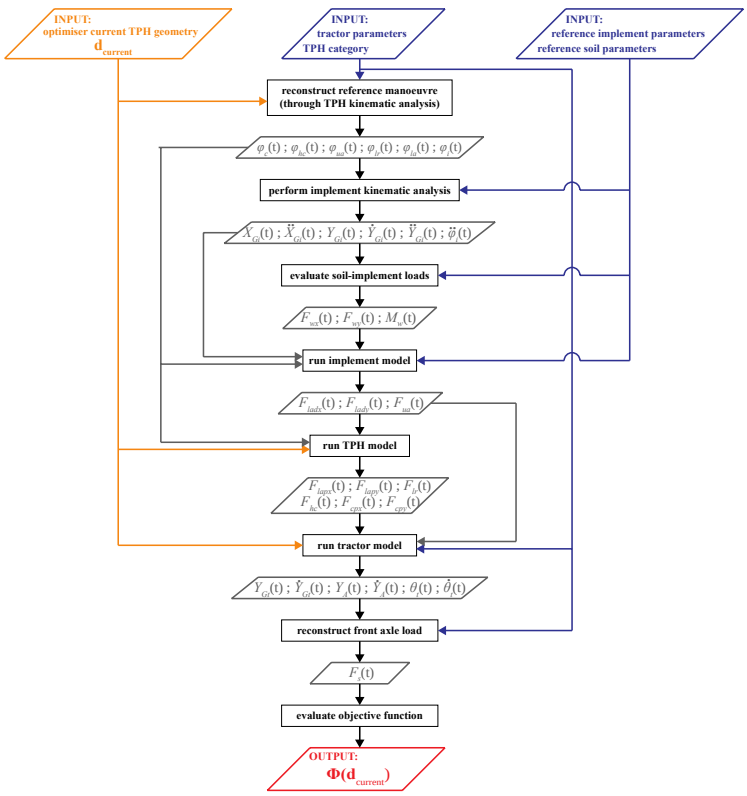

Scheme 2. Algorithm for the evaluation of the objective function to be minimised by the Optimiser. Nomenclature is provided at the end of the paper.

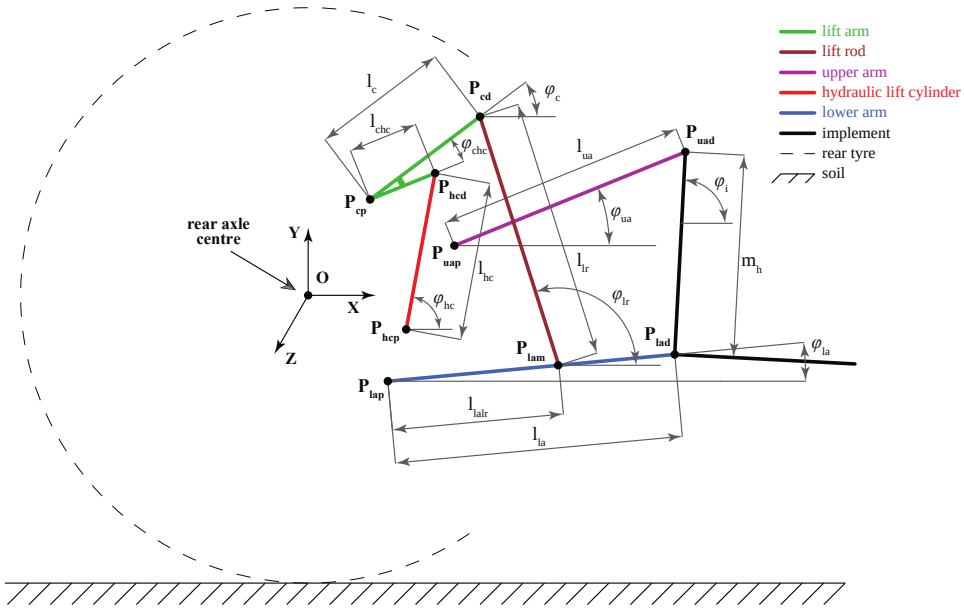

Figure 2. Side view of the TPH and schematic of the implement.

In order for the position analysis of the TPH to be correctly performed, the system of Equation (1) must have six unknowns. Depending on the specific analysis requested at the different stages of the algorithms in Schemes 1 and 2 (e.g., simulating the reference manoeuvre, or enforcing one of the Optimizer nonlinear constraints), the six dimensional parameters playing the role of unknowns may vary.

2.2. Definition of the Reference Manoeuvre

The reference manoeuvre simulates the extraction of a heavy-duty implement (such as a plough or a subsoiler) from the soil and was chosen to trigger weight transfer from the front to the rear axle of the tractor. It was defined in a standardised manner, according to the dimensional requirement of the ISO-730 Standard; in this way, the manoeuvre is adaptable to all the TPH categories. The criteria upon which the manoeuvre is based are the following:

$$\begin{cases} H_{lad,min} = 1.5\ L_{14} \\ H_{lad.max} = H_{lad,min} + 0.2\ L_{18} \\ l_{lr} = l_{lr,max} \\ l_{ua} \text{such that } \varphi_i = \frac{\pi}{2}\ \ at\ H_{lad,min} \end{cases} \tag{2}$$

where $H_{lad,min}$ is the minimum height of the point P_{lad} above the ground (Figure 3a), $H_{lad,max}$ is the maximum height of the point P_{lad} above the ground (Figure 3b), the dimensions l_{lr}, l_{ua}, φ_i are depicted in Figure 2, and the dimensions L_{14} and L_{18} are, respectively, the lower hitch point height and the movement range, as defined by the ISO-730 Standard. Based on criteria (2), the simulated manoeuvre is performed setting the lift rods at their maximum extension and the upper arm in such a way that the implement mast is vertical when the implement is at its minimum height (Figure 3a). This is not a common TPH setup for real applications; however, it was defined in this way for the sake of robustness of the Optimizer: the manoeuvre defined in (2) can be successfully performed with any TPH trial geometries the optimiser might consider during the automated optimisation process.

Through the kinematic analysis of the TPH (system of Equation (1)), the values of the hydraulic lift cylinders length when the TPH is at its lower and higher height, namely $l_{hc,\ min}$ and $l_{hc,max}$, are determined. Then, the speed at which the reference manoeuvre is performed is set by prescribing the extension law of the hydraulic lift cylinders (Figure 3c) as follows:

$$l_{hc}(t) = \frac{l_{hc,\ max} - l_{hc,\ min}}{2} \cdot \mathrm{erf}\left(\frac{t - t_0}{T}\right) + \frac{l_{hc,\ max} + l_{hc,min}}{2} \tag{3}$$

where erf is the Gauss error function, T is a characteristic time to be set based on the flow rate of the hydraulic circuit actuating the hydraulic lift cylinders, t_0 is an offset time for setting the manoeuvre onset, and t is the simulation elapsed time. The choice of the erf function to model the cylinders extension is based on experimental observations (Section 3).

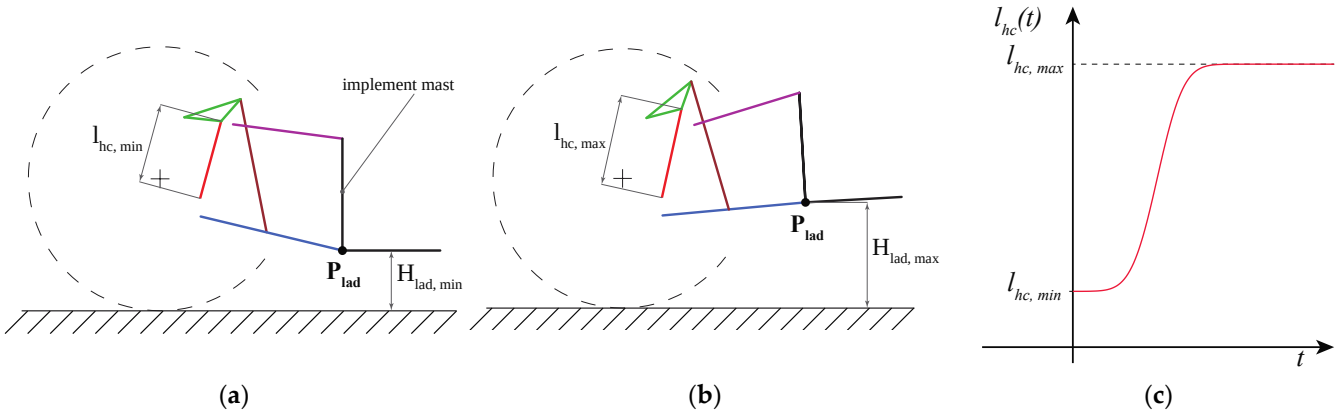

Figure 3. Reference manoeuvre: (**a**) TPH at lower height; (**b**) TPH at higher height; (**c**) hydraulic lift cylinders extension law.

Once the hydraulic lift cylinders extension law is set, a second kinematic analysis is performed to determine the following quantities (Scheme 2):

$$\{\varphi_c(t),\ \varphi_{hc}(t),\ \varphi_{ua}(t),\ \varphi_{lr}(t),\ \varphi_{la}(t),\ \varphi_i(t)\}. \tag{4}$$

In this way, the position of each link of the TPH during the entire reference manoeuvre is completely known.

2.3. Kinematic Analysis of the Implement

Knowing, from (4), the values of the angles φ_{la} and φ_i, the position of the implement COG, G_i, can be determined:

$$\begin{cases} X_{G_i} = X_{P_{lad}} + R_i \sin(\gamma_i + \varphi_i) = X_{P_{lap}} + l_{la}\cos(\varphi_{la}) + R_i \sin(\gamma_i + \varphi_i) \\ Y_{G_i} = Y_{P_{lad}} - R_i \cos(\gamma_i + \varphi_i) = Y_{P_{lap}} + l_{la}\sin(\varphi_{la}) - R_i \cos(\gamma_i + \varphi_i) \end{cases} \tag{5}$$

R_i and γ_i being the polar coordinates of the implement COG with respect to point P_{lad} (Figure 4) and having computed the coordinates of P_{lad} according to the TPH geometry in Figure 2.

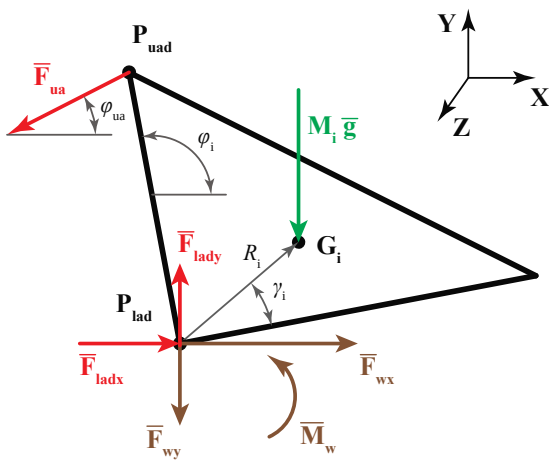

Figure 4. Implement model. Green line: implement weight; brown lines: soil–implement equivalent system of forces; red lines: TPH–implement forces.

To complete the kinematic analysis of the implement (Scheme 2), the first-order and second-order derivatives of X_{G_i}, Y_{G_i}, and φ_i are computed using the central finite difference scheme.

2.4. Soil–Implement Interaction

Since the implement is assumed to behave as a rigid body, the forces exerted by the soil can be represented (Figure 4) as an equivalent system of forces composed by a horizontal force (F_{wx}) and a vertical force (F_{wy}) applied to a reference point of the system, plus a moment (M_w). The point P_{lad} was chosen as the reference point.

The forces exchanged between the soil and the implement depend on constitutive parameters like the geometry of the tillage tools and the soil composition and condition, as well as on operational parameters like the working depth and tractor speed [18–23]. Since the Optimizer simulates a reference manoeuvre performed with a reference implement on a reference soil, and with the tractor moving at constant speed, the forces exerted by the soil on the implement may be assumed to vary only as functions of the working depth and of the implement vertical speed, while all the other parameters remain constant. Hence, the following relations are assumed:

$$\begin{cases} F_{wx} = F_{0x} + K_{sx} \cdot Y_{P_{lad}} \\ F_{wy} = F_{0y} + K_{sy} \cdot Y_{P_{lad}} + C_{sy} \cdot \dot{Y}_{G_i} \\ M_w = M_0 + K_{sm} \cdot Y_{P_{lad}} \end{cases} \tag{6}$$

where F_{0x}, F_{0y}, and M_0 are offset values accounting for the fact that $Y_{P_{lad}}$ is not zero when the implement tools approach the soil, while K_{sx}, K_{sy}, and K_{sm} are proportionality coefficients and C_{sy} is a viscous coefficient defined as:

$$C_{sy} = \begin{cases} C_{sy}^{-}, \text{ if } \dot{Y}_{G_i} \leq 0 \\ C_{sy}^{+}, \text{ if } \dot{Y}_{G_i} > 0 \end{cases} \tag{7}$$

in order to account for the fact that soil drag between implement penetration and extraction is different. The exact values of the coefficients appearing in Equations (6) and (7) were determined at the model validation stage (Section 3).

Many studies report a nonlinear dependence of the soil loads on the working depth [23–26]; however, for the sake of simplicity and without loss of generality, a linear dependence is chosen here.

2.5. Tractor–TPH–Implement Model

The equations of motion for the implement read (Figure 4):

$$\begin{cases} F_{ladx} - F_{ua}\cos(\varphi_{ua}) + F_{wx} - M_i\,\ddot{X}_{G_i} = 0 \\ F_{lady} - F_{ua}\,\sin(\varphi_{ua}) - F_{wy} - M_i\,g - M_i\,\ddot{Y}_{G_i} = 0 \\ -F_{ladx}\,R_i\,\cos(\varphi_i + \gamma_i) - F_{lady}\,R_i\,\sin(\varphi_i + \gamma_i) \\ \qquad +F_{ua}[m_h\sin(\varphi_i - \varphi_{ua}) + R_i\,\cos(\varphi_i - \varphi_{ua} + \gamma_i)] + M_w \\ \qquad -F_{wx}\,R_i\cos(\varphi_i + \gamma_i) + F_{wy}\,R_i\,\sin(\varphi_i + \gamma_i) - I_i^{Gz}\,\ddot{\alpha}_i = 0 \end{cases} \tag{8}$$

where F_{ua} is the force exerted by the TPH upper arm on the implement, F_{ladx} and F_{lady} are, respectively, the horizontal and vertical components of the forces exchanged by the implement and the TPH at the two lower hitch points, M_i is the implement mass, and I_i^{Gz} its moment of inertia with respect to an axis parallel to Z and passing through G_i (Figure 4). g is the gravitational acceleration. Note that the force F_{ua} lies in the same direction as the upper arm.

Once the kinematic analysis of the implement has been performed and the soil–implement loads have been computed, the values of F_{ladx}, F_{ladx} and F_{ua} as functions of time

during the entire reference manoeuvre are determined from the system of Equation (8) (Scheme 2).

As regards the TPH model, it is sufficient to write equilibrium equations for the lower arms (Figure 5a) and for the lift arms (Figure 5b), as inertial effects of the TPH links have been neglected:

$$\begin{cases} F_{lapx} + F_{lr}\cos(\varphi_{lr}) - F_{ladx} = 0 \\ F_{lapy} + F_{lr}\sin(\varphi_{lr}) - F_{lady} = 0 \\ F_{lr}\, l_{lalr}\sin(\varphi_{lr} - \varphi_{la}) - F_{lady}\, l_{la}\cos(\varphi_{la}) + F_{ladx}\, l_{la}\, sin(\varphi_{la}) = 0 \end{cases} \tag{9}$$

where F_{lapx} and F_{lapy} are, respectively, the horizontal and vertical components of the force that the tractor exerts on the TPH through the two lower link points, and F_{lr} is the force acting on the two lower arms due to the lift rods. The force F_{lr} lies in the same direction as the lift rods, and the inclination of the lift rods in the vertical–transversal plane (Y-Z plane, Figure 2) has been neglected for simplicity.

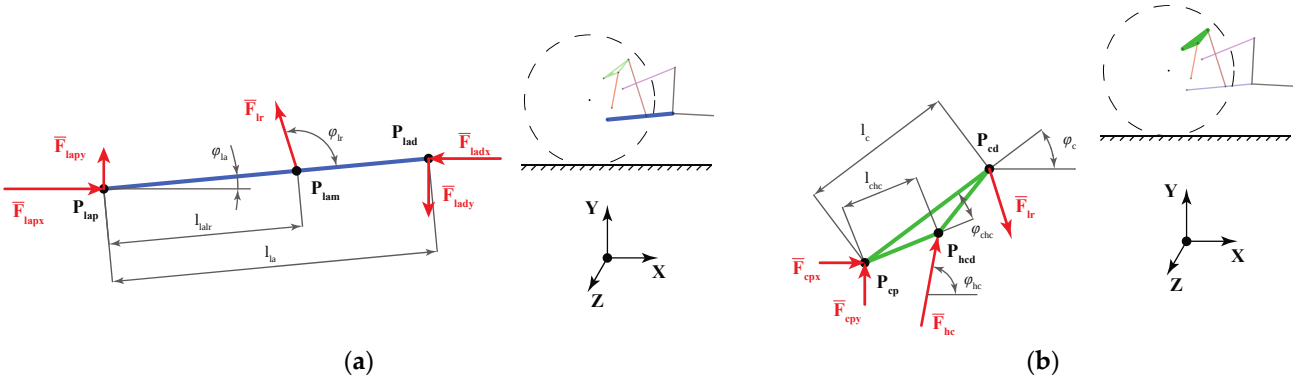

Figure 5. TPH model. (**a**) Lower arms; (**b**) lift arms.

The equilibrium equations of the lift arms read:

$$\begin{cases} F_{cpx} + F_{hc}\cos(\varphi_{hc}) - F_{lr}\cos(\varphi_{lr}) = 0 \\ F_{cpy} + F_{hc}\sin(\varphi_{hc}) - F_{lr}\sin(\varphi_{lr}) = 0 \\ F_{hc}\, l_{chc}\sin(\varphi_{hc} - \varphi_c + \varphi_{chc}) - F_{lr}\, l_c\sin(\varphi_{lr} - \varphi_c) = 0 \end{cases} \tag{10}$$

where F_{cpx} and F_{cpy} are, respectively, the horizontal and vertical components of the force that the tractor exerts on the TPH through the two lift arm link points, and F_{hc} is the force exerted by the two hydraulic lift cylinders on the TPH, lying in the direction of the cylinders. From the systems of Equations (9) and (10), the forces F_{lapx}, F_{lapy}, F_{lr}, F_{cpx}, F_{cpy}, and F_{hc} as functions of time during the entire reference manoeuvre can be calculated (Scheme 2).

As regards the tractor, a 3-degrees-of-freedom model was developed (Figure 6a), taking the vertical displacement of the tractor COG Y_{G_t}, the pitch angle θ_t, and vertical displacement of the front axle unsuspended mass Y_a as the degrees of freedom.

Naming P_{tf} the link points of the front axle suspension on the tractor chassis, P_{tr} the rear wheels hub, and in accordance with the hypotheses on which the model lays (Section 2), the front tyres, the rear tyres, and the front axle suspension transmit the following visco–elastic forces, respectively:

$$F_{fw} = k_f Y_a + c_f\, \dot{Y}_a \tag{11}$$

$$F_{rw} = k_r Y_{tr} + c_r\, \dot{Y}_{tr} \tag{12}$$

$$F_s = k_s\left(Y_{tf} - Y_a\right) + c_s\left(\dot{Y}_{tf} - \dot{Y}_a\right) \tag{13}$$

where k_f, k_r, and k_s are spring constants; c_f, c_r, and c_s are damping coefficients; and Y_{tf}, Y_{tr} are the vertical displacements of the points P_{tf} and P_{tr}, which can be calculated as the

sum of two contributions: the displacement induced by the tractor COG vertical motion and the vertical displacement induced by the pitch motion of the tractor (Figure 6b):

$$Y_{tf} = Y_{G_t} + h_f(1 - \cos\theta_t) - l_f \sin\theta_t \tag{14}$$

$$Y_{tr} = Y_{G_t} + h_r(1 - \cos\theta_t) + l_r \sin\theta_t \tag{15}$$

where h_f, h_r, l_f, and l_r are the dimensions depicted in Figure 6.

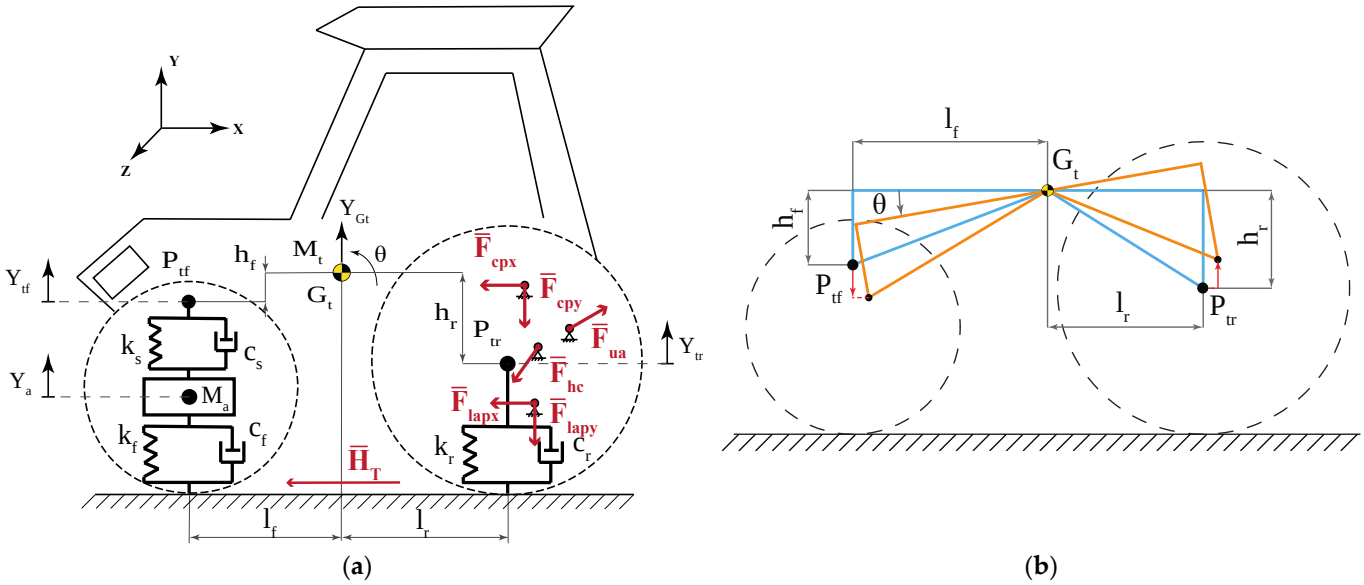

Figure 6. (**a**) The tractor model with the external loads acting on it; (**b**) displacement of the points P_{tf} and P_{tr} due to the sole pitch motion of the tractor.

By taking the derivatives of Equations (14) and (15), the expressions for the vertical velocity of P_{tf} and P_{tr} are obtained:

$$\dot{Y}_{tf} = \dot{Y}_{G_t} + \dot{\theta}_t \left(h_f \sin\theta_t - l_f \cos\theta_t\right) \tag{16}$$

$$\dot{Y}_{tr} = \dot{Y}_{G_t} + \dot{\theta}_t \left(h_r \sin\theta_t + l_r \cos\theta_t\right). \tag{17}$$

The resulting equations of motion for the tractor model are:

$$\begin{cases} M_a \ddot{Y}_a = F_s - F_{fw} - M_a g \\ M_t \ddot{Y}_{G_t} = -F_s - F_{rw} + F_{ua} \sin\varphi_{ua} - F_{lapy} - F_{cpy} - F_{hc} \sin\varphi_{hc} - M_t g \\ I_t^{Gz} \ddot{\theta}_t = F_s\, l_f - F_{rw}\, l_r + F_{ua}\left[\left(l_r + X_{P_{uap}}\right)\sin\varphi_{ua} + \left(h_r - Y_{P_{uap}}\right)\cos\varphi_{ua}\right] - F_{cpy}\left(l_r + X_{P_{cp}}\right) + \\ \qquad -F_{cpx}\left(h_r - Y_{P_{cp}}\right) - F_{hc}\left[\left(l_r + X_{P_{hcp}}\right)\sin\varphi_{hc} + \left(h_r - Y_{P_{fhc}}\right)\cos(\varphi_{hc})\right] + \\ \qquad -F_{lapy}\left(l_r + X_{P_{lap}}\right) - F_{lapx}\left(h_r - Y_{P_{lap}}\right) - H_T\left(h_r + r_{rw} + Y_{tr}\right) \end{cases} \tag{18}$$

where M_a is the front axle unsuspended mass, M_t is the tractor chassis mass, I_t^{Gz} its moment of inertia with respect to an axis parallel to Z and passing through G_t (Figure 6a), H_T is the total traction force developed at the interface between the soil and the tractor wheels, and r_{rw} is the static loaded radius of the rear wheels. As it concerns the third equation in the system (18), considering the total traction force H_T is equivalent to considering the traction forces and the driving torques at the wheel hubs. However, using H_T in the calculation is easier, as there is no need to determine how traction forces and driving torques are distributed between the front and rear wheels.

The total traction force can be determined through the balance of linear momentum of the tractor along the horizontal direction. Since the tractor is assumed to move forward on a straight line at constant speed, the acceleration of the tractor COG is null along the

horizontal direction, and the balance of linear momentum reduces to an equilibrium of the horizontal components of the forces acting on the system, from which H_T can be obtained (Figure 6a):

$$H_T = F_{ua} \cos \varphi_{ua} - F_{hc} \cos \varphi_{hc} - F_{lapx} - F_{cpx} \,. \tag{19}$$

Upon substituting Equations (11)–(13) and (19) into (18), and accounting for Equations (14)–(17), a system of three-second order ODEs is obtained, which constitutes the tractor model in the algorithm depicted in Scheme 2. The values of the loads exerted by the TPH on the tractor during the entire reference manoeuvre are known from the previous steps of the algorithm, and solving the system of Equation (18) allows to determine the quantities:

$$\{Y_a(t),\ Y_{G_t}(t),\ \theta_t(t)\} \,. \tag{20}$$

The system of Equation (18) is solved using an explicit Runge–Kutta method through the MATLAB built-in function *ode45* (MATLAB®, Mathworks, Inc., Natick, MA, USA).

Once the values of the quantities (20) have been determined, the load on the tractor front axle as a function of time during the entire reference manoeuvre can be reconstructed (Scheme 2). Accounting for Equations (13), (14), and (16), the front axle load takes the form:

$$F_s = k_s\left(Y_{G_t} + h_f(1-\cos\theta_t) - l_f \sin\theta_t - Y_a\right) + c_s\left(\dot{Y}_{G_t} + \dot{\theta}_t\left(h_f \sin\theta_t - l_f \cos\theta_t\right) - \dot{Y}_a\right) \tag{21}$$

2.6. Optimiser

The Optimiser solves the following mathematical problem (Scheme 1):

$$\begin{cases} \min\limits_{d} \Phi(d) \\ C_k(d) \le 0,\ k = 1, \cdots, N_C \\ L_j \le d_j \le U_j,\ j = 1, \cdots,\ N_D \end{cases} \tag{22}$$

where d is a vector containing all the TPH dimensions subject to optimisation, Φ is the objective function to be minimised, C_k are the constraints that the TPH has to satisfy, N_C is the number of constraints, L_j and U_j are, respectively, the lower and upper bounds on the dimension d_j, and N_D is the number of TPH dimensions subject to optimisation. The dimensions vector is composed by $N_D = 19$ TPH dimensions, namely:

$$d = \left[X_{P_{cp}}; Y_{P_{cp}}; X_{P_{hcp}}; Y_{P_{hcp}}; X_{P_{lap}}; Y_{P_{lap}}; X_{P_{uap}}; Y_{P_{uap}}; l_c; l_{chc}; l_{la}; l_{lalr}; l_{lr_{max}}; l_{lr_{min}}; l_{ua_{max}}; l_{ua_{min}}; \varphi_{chc}; \varphi_{c_{max}}; \varphi_{c_{min}}\right]$$

The objective function is the peak-to-peak (P2P) value of the front axle load (Equation (21)) during the reference manoeuvre and is determined through the algorithm depicted in Scheme 2:

$$\Phi = \mathrm{P2P}(F_s) \,. \tag{23}$$

Ensuring that the optimiser minimises $\Phi(d)$ will result in finding the TPH optimal geometry, which minimises the weight-transfer effect during the reference manoeuvre. Problem (22) is solved using an active-set sequential quadratic programming method through the MATLAB built-in function *fmincon* (MATLAB®, Mathworks, Inc., Natick, MA, USA).

2.6.1. Optimiser Constraints

The Optimiser accounts for $N_C = 36$ constraints (Table 1), implemented in the non-dimensional form $C_k(x) \le 0$. For the sake of readability, constraints will not be presented in this form in Table 1, but in the form they were naturally derived.

Constraints C1–C3 are logical constraints on some of the elements of d: for obvious reasons, the maximum extension of the lift rods and of the upper arm cannot be less than their minimum extension; similarly, the maximum value of the lift arms angle cannot be less than its minimum value. Constraints C4–C10 are robustness constraints: they prescribe conditions for the existence of the closed polygons, which constitute the TPH kinematic subsystems described in Section 2.1, thus impeding the Optimiser from choosing

trial geometries that would result in unfeasible TPH mechanisms. Constraints C11–C16 are functional constraints: for manufacturing and accessibility reasons, there needs to be a minimum ensured distance between some link points; moreover, the hydraulic lift cylinders must not reach a vertical position when fully extended. Constraints C17–C19 are proportioning constraints on the ratio of minimum to maximum length of the extensible links, set to avoid disproportioning.

Table 1. Optimiser constraints.

Nr.	Equation	Significance
C1	$\varphi_{c,max} \geq \varphi_{c,min}$	Logical constraints
C2	$l_{lr,max} \geq l_{lr,min}$	
C3	$l_{ua,max} \geq l_{ua,min}$	
C4	$l_c + l_{lr,min} + l_{lalr} \geq \lvert P_{lap} - P_{cp} \rvert$	Robustness constraints
C5	$l_{lr,min} + l_{lalr} + \lvert P_{lap} - P_{cp} \rvert \geq l_c$	
C6	$l_c + l_{lr,min} + \lvert P_{lap} - P_{cp} \rvert \geq l_{lalr}$	
C7	$l_c + \lvert P_{lap} - P_{cp} \rvert + l_{lalr} \geq l_{lr,max}$	
C8	$m_h + l_{la} + l_{ua,\,min} \geq \lvert P_{lap} - P_{uap} \rvert$	
C9	$m_h + \lvert P_{lap} - P_{uap} \rvert + l_{ua,\,min} \geq l_{la}$	
C10	$m_h + l_{la} + \lvert P_{lap} - P_{uap} \rvert \geq l_{ua,\,max}$	
C11	$l_c - l_{chc} \geq 50$ mm	Functional constraints
C12	$l_{la} - l_{lalr} \geq 200$ mm	
C13	$Y_{P_{cp}} - Y_{P_{lap}} \geq 50$ mm	
C14	$Y_{P_{uap}} - Y_{P_{lap}} \geq 300$ mm	
C15	$Y_{P_{hcp}} - Y_{P_{lap}} \geq 0$ mm	
C16	$\varphi_{hc,\,max} \leq 85°$	
C17	$\frac{l_{hc,\,min}}{l_{hc,max}} \geq 0.6$	Proportioning constraints
C18	$\frac{l_{lr,\,min}}{l_{lr,max}} \geq 0.7$	
C19	$\frac{l_{ua,\,min}}{l_{ua,max}} \geq 0.6$	
C20	$X_{P_{lap}} + l_{la} - X_{PTO} \geq L_{MIN}$	Tractor PTO distance from lower hitch points (ISO-730, Figure 2 and Table 2)
C21	$X_{P_{lap}} + l_{la} - X_{PTO} \leq L_{MAX}$	
C22	$H_{lad,min} \leq L_{14}$	Lower hitch points height, TPH in configuration A (dimension L_{14} as per ISO-730)
C23	$H_{lad,min} \geq 50$ mm	
C24	$\varphi_{lr} \geq 95°$	Functional requirements for TPH in configuration A
C25	$\varphi_i \leq 90°$	
C26	$H_{lad,max} \geq L_{19}$	Transport height, TPH in configuration B (dimension L_{19} as per ISO-730)
C27	$\Delta_{min} \geq L_{20}$	Lower hitch points clearance, TPH in configuration B (dimension L_{20} as per ISO-730)
C28	$l_{ua} \geq l_{ua,\,min}$	Functional constraints for configuration C
C29	$l_{ua} \leq l_{ua,\,max}$	
C30	$\frac{l_{lr,\,max} + l_{lr,\,min}}{2} \geq l_{lr,\,lim}$	
C31	$L_{CV} \geq 0.9\,(l_f + l_r)$	Constraints on vertical convergence distance
C32	$L_{CV} \leq 3\,(l_f + l_r)$	
C33	$\frac{H_{lad,\,max} - H_{lad,min}}{2} \geq L_{15}$	Levelling adjustment, TPH in configuration C (dimension L_{15} as per ISO-730)
C34	$H_{lad,\,max} - H_{lad,min} \geq L_{18}$	Movement range, TPH from configuration D_1 to D_2 (dimension L_{18} as per ISO-730)
C35	$\varphi_{i,\,max} \geq$ 95° (90° for category 1N TPH)	Mast adjustment, TPH in configurations E_1 and E_2 (ISO-730, comma 3.2.22)
C36	$\varphi_{i,\,min} \leq$ 85° (80° for category 1N TPH)	

The other constraints are derived from the requirements contained in the ISO-730 Standard: constraints C20–C21 account for the tractor power take-off (PTO) location with respect to the TPH, while constraints C22–C36 concern the functional performance of the TPH and are enforced by evaluating, through the kinematic analysis described in Section 2.1, the TPH geometry in the different configurations described in Appendix A.

3. Model Validation

To validate the soil–implement interaction model and to determine the values of the coefficients in Equations (6) and (7), a series of tests was conducted (Figure 7) in which a tractor with a sensorised TPH performed a manoeuvre similar to the reference manoeuvre described in Section 2.2. Tests were performed on a clay–loam untilled soil, in a farm located in northern Italy. The tractor used for the tests was a 96 kW MFWD tractor with a rear-mounted category 3 TPH. A 7-shank subsoiler (Table 2) was attached to the tractor and the loads at different locations of the TPH were measured during implement manoeuvring. The tractor was equipped with the following sensors: a pressure sensor mounted on the hydraulic lift cylinders; a load cell placed on the TPH upper arm; a load cell that measured the horizontal component of the force at the lower link points; a sensor for measuring the lift arms angle with respect to the horizontal direction, which allowed to reconstruct the TPH configuration; and a pressure sensor on the front-axle hydropneumatic suspension.

Figure 7. Model validation tests setup: a 7-shanks subsoiler is connected to the rear TPH of the tractor.

Table 2. Implement used in the validation tests.

Implement Type Number of Tools	Subsoiler 7 Shanks
M_i	768 kg
I_i^{Gz}	314 kg m^2
R_i	795 mm
γ_i	5.19°
m_h	690 mm

The manoeuvre consisted of raising and lowering the subsoiler while the tractor was running at a constant speed of 2 km/h. Several consecutive repetitions of the manoeuvre were performed. For the whole extent of the manoeuvre, the subsoiler shanks were sunk into the ground.

Figure 8 shows a comparison between the measured and simulated TPH configuration in terms of the hydraulic lift cylinders' extension for three test repetitions; the simulated values were determined using Equation (3). It can be observed that the model is able to reproduce the experimental manoeuvre and, in particular, the *erf* function appears to be an effective choice for approximating the cylinder kinematics observed in the field tests.

Figure 9 shows a comparison between the force measured at different locations of the TPH and the force predicted through the soil–implement interaction model in Equations (6) and (7), the implement model in Equation (8), and the TPH model in Equations (9) and (10). From the comparison, it can be concluded that the soil–implement interaction model is suitable for describing the loads that the soil exerts on the subsoiler

shanks during a raising/lowering manoeuvre. In particular, the peak in the hydraulic lift cylinders force during implement extraction from the soil is reproduced. Further analysis shows that such peak is aligned with the peak in the implement vertical speed (Figure 10), suggesting that the loads exerted by the soil on the implement should depend not only on the working depth, but also on the speed of penetration/extraction of the implement into/from the soil. This is the reason that led to the introduction of the viscous term in the expression of F_{wy} in Equation (6).

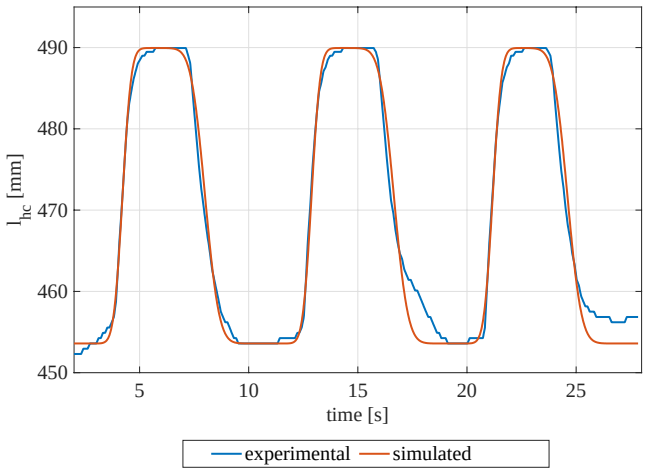

Figure 8. Reconstruction of the hydraulic lift cylinders extension during three manoeuvre repetitions.

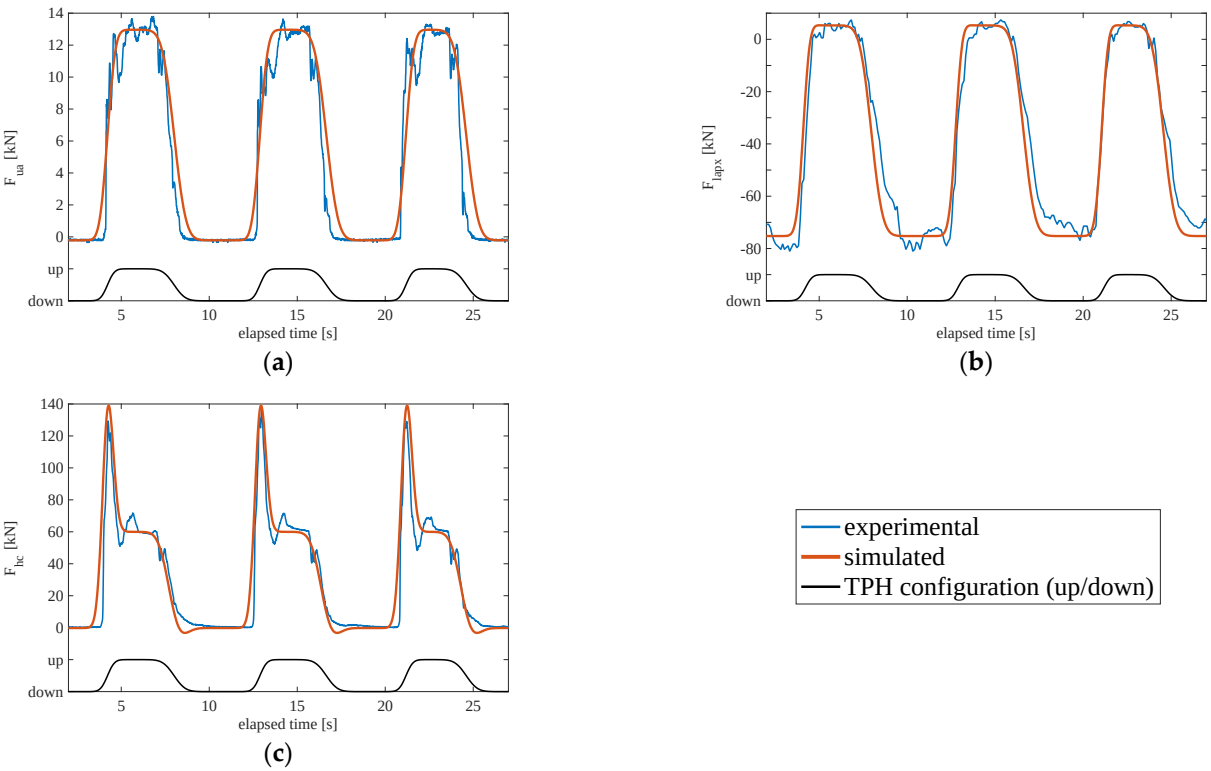

Figure 9. Comparison between experimental and simulated force profile during implement manoeuvring. (**a**) Force at the upper arm; (**b**) force at the lower link points, horizontal component; (**c**) force at the hydraulic lift cylinders.

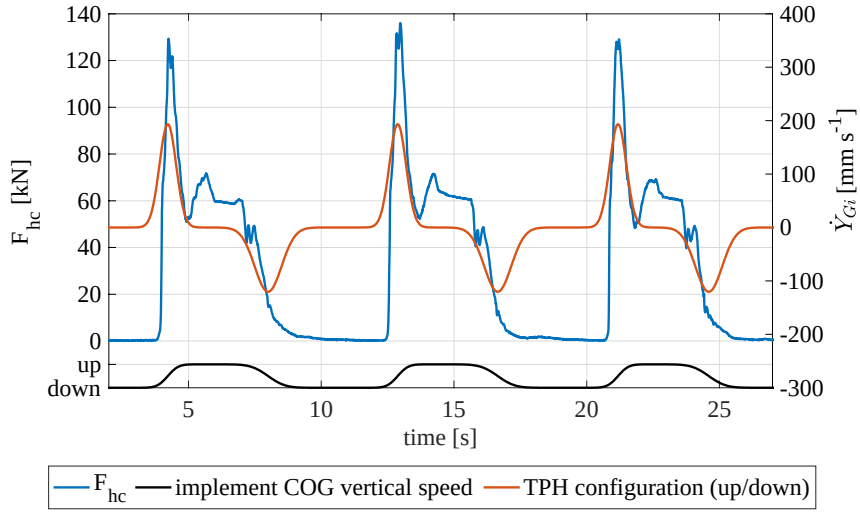

Figure 10. Relationship between the force at the hydraulic lift cylinders and the implement COG vertical speed.

From the field tests, the parameters for the reference manoeuvre and the reference soil were also determined by taking the values that allowed to best match the experimental measurements (Table 3). The subsoiler used in the validation tests was taken as the reference implement for the model.

Table 3. Parameters used in the simulations.

Reference manoeuvre	T	0.444 s
	t_0	5 s
	$Y_{P_{lad}}$, min	−451 mm (TPH down)
	$Y_{P_{lad}}$, max	−304 mm (TPH up)
Reference implement	Table 2	
Reference soil	F_{0x}	−125.9 kN
	F_{0y}	14.23 kN
	M_0	-21.8×10^3 N m
	K_{sx}	0.445 kN mm^{-1}
	K_{sy}	26.4×10^{-3} kN mm^{-1}
	K_{sm}	68.6 kN
	C_{sy}^{-}	65 N s mm^{-1}
	C_{sy}^{+}	140 N s mm^{-1}

4. Results and Discussion

Simulations were performed to show the capabilities of the Optimiser and of the underlying tractor–TPH–implement model. The tractor used for the validation tests was taken as the benchmark for the simulations. As described in Section 2, the Optimiser simulates the reference manoeuvre performed on the reference soil with the reference implement; the values of the manoeuvre, soil, and implement parameters are listed in Table 3. The values of the tractor parameters used in the simulations are listed in Table 4. Spring constants, damping coefficients, and tractor moment of inertia were set through a parameter identification procedure that involved measuring the front axle load during an in-filed manoeuvre similar to the reference manoeuvre, performed with the subsoiler used for the validation tests (Table 2). The parameter identification procedure consisted of choosing the parameters values that allowed to best match the higher and lower peaks in the simulated front axle response with those of the experimental signal. The starting values for the parameter identification procedure were taken from data available in the literature [27–30].

Table 4. Tractor parameters used in the tractor dynamic model.

M_t	5975 kg
I_t^{Gz}	5220 kg m^2
M_a	298 kg
l_f	1069 mm
l_r	1491 mm
h_f	195 mm
h_r	20 mm
r_{rw}	877 mm
k_s	1.10×10^5 N m^{-1}
k_f	1.00×10^6 N m^{-1}
k_r	2.10×10^6 N m^{-1}
c_s	4.60×10^3 N s m^{-1}
c_f	9.10×10^3 N s m^{-1}
c_r	1.00×10^4 N s m^{-1}

4.1. Behaviour of the Tractor–TPH–Implement Aggregate during the Reference Manoeuvre

The predicted loads exchanged between the soil and the implement during the reference manoeuvre are depicted in Figure 11. It can be observed that the horizontal component F_{wx}, Figure 11a, points rearward, exerting a drag force that reaches its maximum when the working depth of the implement is maximum and decreases as the implement is lifted. As regards the vertical component F_{wy}, Figure 11b, a peak is observed during the reference manoeuvre, which is induced by the behaviour of the implement vertical speed (Figure 10) and by the fact that the soil–implement loads depend on the speed of extraction of the implement from the soil (Equation (6)). The fact that F_{wy} points downward is consistent with the literature [31] and is due to the value of the rake angle of the reference implement shanks, which is smaller than the cross-over value discussed by Goodwin [22,24]. Furthermore, the sign of the moment of the resultant about the point P_{lad}, Figure 11c, indicates that the line of pull lies below P_{lad} when the implement working depth is maximum, whereas when the working depth is minimum, the horizontal component of the resultant decreases significantly, causing the line of pull to move rearward with respect to P_{lad} and, ultimately, the moment M_w to be negative.

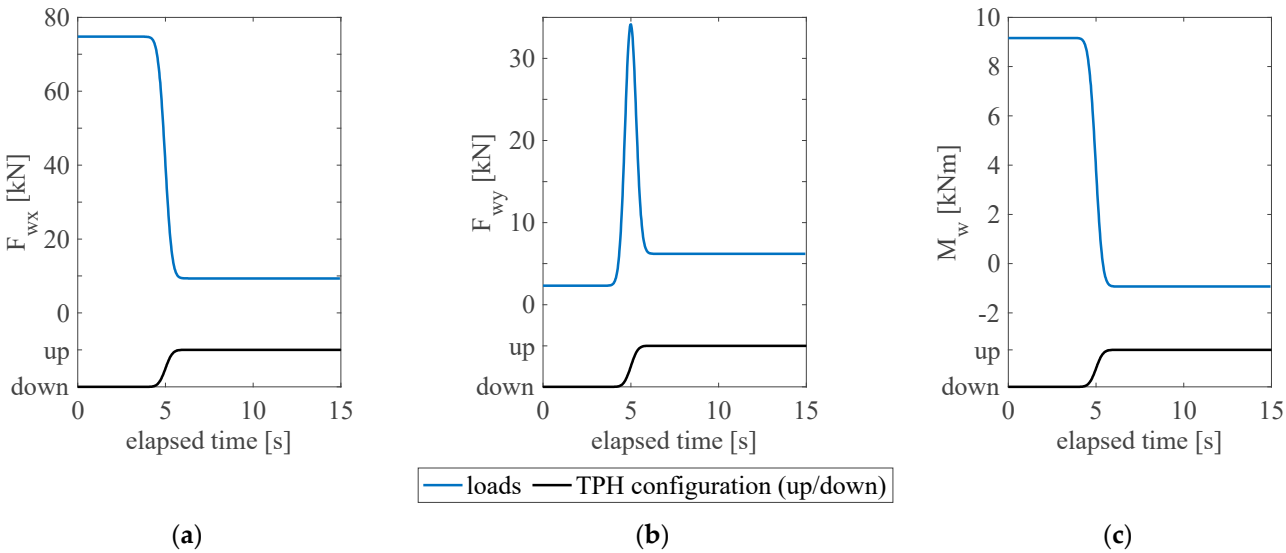

Figure 11. Soil–implement system of forces during the reference manoeuvre: (**a**) horizontal force (positive if rearward); (**b**) vertical force (positive if downward); and (**c**) moment of the resultant about the point P_{lad} (positive if anti-clockwise).

Figure 12 shows the behaviour of the load on the tractor front axle during the reference manoeuvre. It can be observed that lifting the implement causes the load on the front axle to decrease drastically. This is ultimately due to the peak in the vertical force F_{wy} (Figure 11b). At the end of the manoeuvre, the front axle load exhibits an overshoot, and then a damped oscillation occurs, due to the viscoelastic nature of tyres and front axle suspension. After oscillations are dampened out, the front axle load reaches a higher value compared to the beginning of the manoeuvre, as the implement drag is lower at the end of the manoeuvre than at the beginning (Figure 11). The reference manoeuvre thus proves to be effective in inducing weight transfer from the front to the rear axle and the P2P value of the force on the front axle appears to be a suitable measure of this phenomenon.

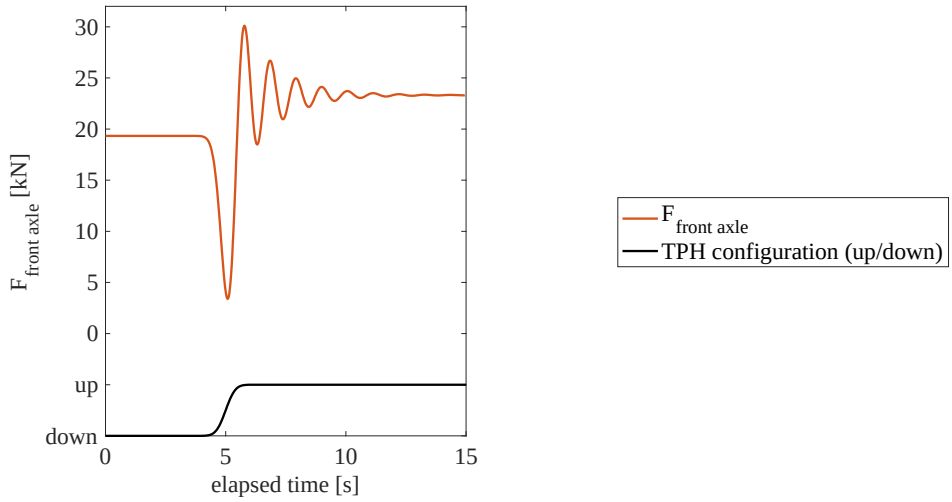

Figure 12. Simulated front axle response due to the reference manoeuvre performed with the reference implement on the reference soil.

4.2. TPH Optimisation

To test the capabilities of the Optimiser, the geometry of a commercially available category 3 TPH was chosen as the initial TPH geometry (Scheme 1). Design considerations led to establish lower and upper bounds on the TPH dimensions subject to optimisation (Table 5), which were imposed on the Optimiser (Problem 22). The constraints listed in Table 1 were enforced, setting the limit values prescribed by the ISO-730 Standard for a category 3 TPH (Table 6).

Table 7 summarises the performance of the Optimizer: after 36 iterations, an optimised TPH geometry was found that allowed to reduce the P2P value of the front axle load by 14.9%. A comparison between the initial and optimised TPH geometry is shown in Figure 13. In the optimised geometry, the point P_{lap} is shifted towards the rear axle centre as much as the bounds on the dimensions $X_{P_{lap}}$ and $Y_{P_{lap}}$ allowed. Furthermore, the point P_{cp} is shifted upward and rearward, while the angle φ_{chc} is considerably smaller than it was in the starting TPH geometry; as a consequence, the value of the dimension $\varphi_{c_{min}}$ decreased to its lower admissible value. Figure 13 also shows that the point P_{uap} is considerably shifted upward and rearward, the value of the dimension $X_{P_{uap}}$ being equal to its upper admissible value.

Table 5. Lower and upper bounds on the TPH dimensions subject to optimisation.

TPH Dimension	Lower Bound	Upper Bound	Unit
$X_{P_{cp}}$	140	200	mm
$Y_{P_{cp}}$	325	475	mm
$X_{P_{hcp}}$	235	300	mm
$Y_{P_{hcp}}$	−150	−90	mm
$X_{P_{lap}}$	50	280	mm
$Y_{P_{lap}}$	−270	−180	mm
$X_{P_{uap}}$	275	475	mm
$Y_{P_{uap}}$	200	550	mm
l_c	300	500	mm
l_{chc}	150	350	mm
l_{la}	500	1500	mm
l_{lalr}	250	1000	mm
$l_{lr_{min}}$	400	1200	mm
$l_{lr_{max}}$	400	1200	mm
$l_{ua_{min}}$	400	1200	mm
$l_{ua_{max}}$	400	1200	mm
φ_{chc}	10	45	°
$\varphi_{c_{max}}$	30	80	°
$\varphi_{c_{min}}$	−20	50	°

Table 6. ISO-730 functional prescriptions for a category 3 TPH (Section 2.6.1 and Table 1).

L_{min}	560	mm
L_{max}	775	mm
L_{14}	230	mm
L_{15}	125	mm
L_{18}	735	mm
L_{19}	1065	mm
L_{20}	100	mm
$H_{ma,\ min}$	230	mm
$H_{ma,\ max}$	660	mm

Table 7. Optimiser performance.

$\Phi_{initial}$	27.07	kN
$\Phi_{optimised}$	23.05	kN
reduction	14.9	%
no. of iterations	36	

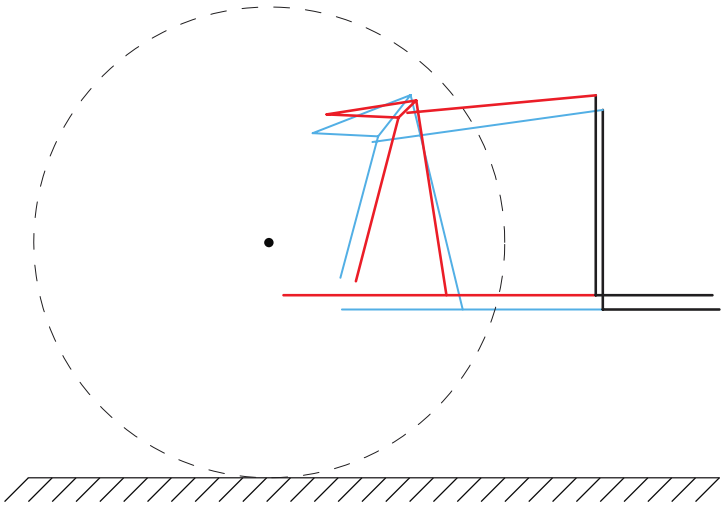

Figure 13. Comparison between the initial (blue lines) and optimised (red lines) TPH geometry.

5. Conclusions

The paper presents a computational tool (the Optimiser) developed to optimise the geometry of a tractor rear-mounted TPH in order to minimise the weight transfer from the front to the rear tractor axle during implement operation or manoeuvring. To this end, the Optimiser simulates a reference manoeuvre performed with a reference implement on a reference soil. Simulations are based on a dynamic model of the tractor–TPH–implement aggregate. The following conclusions can be drawn from the study:

- The proposed reference manoeuvre, defined in a general manner based on ISO-730 functional requirements, is suitable for all TPH categories and can accurately reproduce real infield implement manoeuvring;
- The soil–implement interaction model developed in the study and implemented in the Optimiser was successfully validated against infield test data;
- The reference manoeuvre is effective in triggering the weight-transfer effect and the P2P value of the front axle load during the reference manoeuvre appears to be a suitable measure of this phenomenon;
- The Optimiser was subjected to a benchmark test starting from the geometry of a commercially available TPH; the test showed that the Optimiser was able to find an optimised TPH geometry which allows to reduce the weight-transfer effect by 14.9%.

Author Contributions: Conceptualization, M.M. (Mirko Maraldi) and M.M. (Michele Mattetti); methodology, M.M. (Mirko Maraldi) and M.M. (Michele Mattetti); software, M.M. (Mirko Maraldi) and L.A.F.; validation, M.M. (Mirko Maraldi) and L.A.F.; formal analysis, M.M. (Mirko Maraldi); investigation, M.M. (Mirko Maraldi) and L.A.F.; resources, M.M. (Mirko Maraldi), M.M. (Michele Mattetti) and M.V.; data curation, M.Mar and L.A.F.; writing—original draft preparation, M.M. (Mirko Maraldi) and L.A.F.; writing—review and editing, M.M. (Mirko Maraldi), L.A.F., M.M. (Michele Mattetti), and M.V.; visualization, M.M. (Mirko Maraldi) and L.A.F.; supervision, M.M. (Mirko Maraldi) and M.M. (Michele Mattetti); project administration, M.M. (Michele Mattetti); funding acquisition, M.M. (Michele Mattetti). All authors have read and agreed to the published version of the manuscript.

Funding: This research received no external funding.

Conflicts of Interest: The authors declare no conflict of interest.

Nomenclature

Symbol	Variable	Unit (SI)
c_f	front wheels damping coefficient	N s m^{-1}
C_k	TPH constraint no. k	–
c_r	rear wheels damping coefficient	N s m^{-1}
c_s	front axle suspension damping coefficient	N s m^{-1}
C_{sy}	viscous coefficient for the soil-implement vertical force	N s m^{-1}
d	TPH dimensions vector	–
erf	Gauss error function	–
F_{0x}	offset value for the soil-implement horizontal force	N
F_{0y}	offset value for the soil-implement vertical force	N
F_{cp}	force at the two lift arm link points	N
F_{fw}	front wheels force	N
F_{hc}	hydraulic lift cylinders force	N
F_{lad}	force at the two lower hitch points	N
F_{lap}	force at the two lower link points	N
F_{lr}	lift rods force	N
F_{rw}	rear wheels force	N
F_s	front axle suspension force	N
F_{ua}	upper arm force	N
F_{wx}	soil-implement force, horizontal component	N
F_{wy}	soil-implement force, vertical component	N
g	gravitational acceleration	m s^{-2}

G_i	implement centre of gravity	–
G_t	tractor centre of gravity	–
h_f	vertical distance between tractor centre of gravity and front axle	m
H_{lad}	height of lower hitch points above the ground	m
H_{ma}	height of lower hitch points above the ground	m
h_r	vertical distance between tractor centre of gravity and rear axle	m
H_T	total traction force	N
I_i^{Gz}	implement moment of inertia	kg m^2
I_t^{Gz}	tractor moment of inertia	kg m^2
k_f	front wheels spring constant	N m^{-1}
k_r	rear wheels spring constant	N m^{-1}
k_s	front axle suspension spring constant	N m^{-1}
K_{sm}	proportionality coefficient for the soil-implement moment	N
K_{sx}	proportionality coefficient for the soil-implement horizontal force	N m^{-1}
K_{sy}	proportionality coefficient for the soil-implement vertical force	N m^{-1}
L	distance between power take-off and lower hitch points	m
L_{14}	lower hitch point height as per ISO-730	m
L_{15}	levelling adjustment as per ISO-730	m
L_{18}	movement range as per ISO-730	m
L_{19}	transport height as per ISO-730	m
L_{20}	lower hitch point clearance as per ISO-730	m
l_c	lift arm length	m
l_{chc}	lift arm cranks length	m
L_{CV}	vertical convergence distance	m
l_f	longitudinal distance between tractor centre of gravity and front axle	m
l_{hc}	hydraulic lift cylinders length	m
L_j	lower bound on dimension d_j	various
l_{la}	lower arm length	m
l_{lalr}	distance of the lift rods link on the lower arms	m
l_{lr}	lift rods length	m
l_r	longitudinal distance between tractor centre of gravity and rear axle	m
l_{ua}	upper arm length	m
M_0	offset values for the soil-implement moment	N m
M_a	front axle unsuspended mass	kg
m_h	mast height	m
M_i	implement mass	kg
M_t	tractor chassis mass	kg
M_w	moment of the soil-implement resultant about point P_{lad}	N m
N_C	number of TPH constraints	–
N_D	number of TPH dimensions subject to optimisation	–
P_{cd}	lift arm—lift rod connection points	–
P_{cp}	lift arm link points	–
P_{hcd}	lift arm—hydraulic lift cylinder connection points	–
P_{hcp}	hydraulic lift cylinder link point	–
P_{lad}	lower hitch points	–
P_{lam}	lift rod—lower link connection points	–
P_{lap}	lower link points	–
P_{tf}	link point of front axle suspension on the tractor chassis	–
P_{tr}	link point of rear wheels hubs on the tractor chassis	–
P_{uad}	upper hitch point	–
P_{uap}	upper link point	–
R_i	radial coordinate of the implement centre of gravity	m
r_{rw}	static loaded radius of the rear wheels	m
T	reference manoeuvre characteristic time	s
t	simulation elapsed time	s
t_0	offset time for reference manoeuvre onset	s
U_j	upper bound on dimension d_j	various
X_{P_k}	longitudinal coordinate of the point P_k	m
X_{PTO}	power take-off length	m

Y_a	front axle unsuspended mass vertical displacement	m
Y_{P_k}	vertical coordinate of the point P_k	m
γ_i	angular coordinate of the implement centre of gravity	rad
Δ_{min}	lower hitch points clearance	m
θ_t	tractor pitch angle	rad
Φ	objective function	N
φ_c	lift arm angle	rad
φ_{chc}	lift arms crank angle	rad
φ_{hc}	hydraulic lift cylinder angle	rad
φ_i	implement mast angle	rad
φ_{la}	lower arm angle	rad
φ_{lr}	lift rod angle	rad
φ_{ua}	upper arm angle	rad

Appendix A

The constraints on the TPH geometry derived from the ISO-730 requirements and listed in Table 1 are enforced by evaluating, through the kinematic analysis described in Section 2.1, the TPH geometry in the different configurations depicted in Figure A1 and described in this Appendix.

Configuration A (Figure A1a)

It has the following features:

- Lift rods set at maximum length: $l_{lr} = l_{lr,\ max}$;
- Upper arm set at maximum length: $l_{ua} = l_{ua,\ max}$;
- Hydraulic lift cylinders fully closed: $l_{hc} = l_{hc,\ min}$; i.e., lift arms at minimum angle: $\varphi_c = \varphi_{c,\ min}$.

From this configuration, the lower hitch points height above the ground $H_{lad,\ min}$ depicted in Figure A1a is deduced, and constraints C22–23 are enforced. Constraints C24 and C25 are additional functional requirements prescribing that the lift rods must not be close to the vertical position and that the implement is inclined rearward in this configuration.

Configuration B (Figure A1b)

It has the following features:

- Lift rods set at minimum length: $l_{lr} = l_{lr,\ min}$;
- Upper arm set at intermediate length: $l_{ua} = \frac{l_{ua,\ max}+l_{ua,\ min}}{2}$;
- Hydraulic lift cylinders fully extended: $l_{hc} = l_{hc,\ max}$; i.e., lift arms at maximum angle: $\varphi_c = \varphi_{c,\ max}$.

This configuration is used to enforce constraint C26 on the transport height $H_{lad,\ max}$ depicted in Figure A1b and constraint C27 on the lower hitch points clearance Δ_{min}. Both the transport height and lower hitch point clearance are defined by the ISO-730 Standard, the latter being calculated as follows:

$$\Delta_{min} = \sqrt{\left(X_{P_{lap}} + l_{la}\cos\varphi_{la}\right)^2 + \left(Y_{P_{lap}} + l_{la}\sin\varphi_{la}\right)^2} - r_{rw} \tag{A1}$$

Configuration C (Figure A1c)

It has the following features:

- Lift rods set at intermediate length: $l_{lr} = \frac{l_{lr,\ max}+l_{lr,\ min}}{2}$;
- Horizontal lower arms: $\varphi_{la} = 0°$;
- Vertical implement mast: $\varphi_i = 90°$.

The length at which the upper arm needs to be set in configuration C is:

$$l_{ua} = \sqrt{\left(X_{P_{lap}} + l_{la} - X_{P_{uap}}\right)^2 + \left(Y_{P_{lap}} + m_h - Y_{P_{uap}}\right)^2} \tag{A2}$$

while the minimum value of lift rod length that allows to have horizontal lower arms is:

$$l_{lr,\,lim} = \sqrt{\left(X_{P_{lap}} + l_{lalr} - X_{cp} - l_c \cos\varphi_{c,\,min}\right)^2 + \left(Y_{P_{cp}} + l_c \sin\varphi_{c,\,min} - Y_{P_{lap}}\right)^2} \tag{A3}$$

To ensure that configuration C can be obtained, constraints C28–C30 are enforced: constraints C28 and C29 ensure that the length l_{ua} in Equation (A2) falls within the minimum and maximum upper arm length, while constraint C30 ensures that the intermediate lift rods length is greater than the limit value determined through Equation (A3).

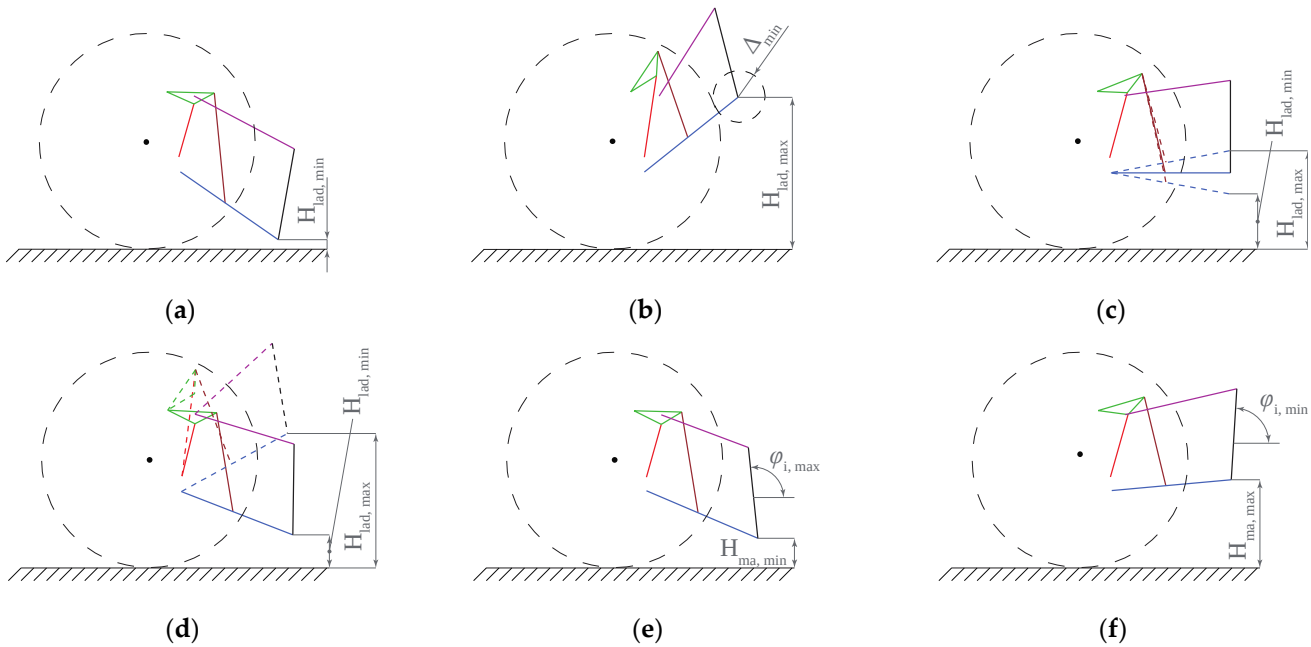

Figure A1. TPH configurations used to enforce constraints C22–C36 (Table 1).

From configuration C, the vertical convergence distance L_{CV} of the TPH (ISO-730, 2009) can be calculated by observing that:

$$\frac{L_{CV}}{X_{P_{lap}} + l_{la} - X_{P_{uap}}} = \frac{m_h}{m_h - \left(Y_{P_{uap}} - Y_{P_{lap}}\right)},$$

which leads to:

$$L_{CV} = m_h \frac{X_{P_{lap}} + l_{la} - X_{P_{uap}}}{m_h - Y_{P_{uap}} + Y_{P_{lap}}}. \tag{A4}$$

Once L_{CV} is determined, constraints C31 and C32 can be enforced: the former is prescribed by the ISO-730 Standard, while the latter represents an upper limit on L_{CV} and is set for design reasons.

Configuration C is also used to enforce constraint C33 on the levelling adjustment required by the ISO-730 Standard. This is done by evaluating the heights $H_{lad,\,min}$ and $H_{lad,\,max}$ of the lower hitch points above the ground (Figure A1c). $H_{lad,\,min}$ is obtained starting from configuration C and fully extending one lift rod, while $H_{lad,\,max}$ is found starting from configuration C and shortening one lift rod to its minimum length.

Configuration D1 and D2 (Figure A1d)

These configurations are used to enforce the constraint C34 on the movement range required by the ISO-730 Standard and are reached with the following TPH setup:

- Lift rods set at intermediate length: $l_{lr} = \frac{l_{lr,\ max}+l_{lr,\ min}}{2}$;
- Upper arm set at intermediate length: $l_{ua} = \frac{l_{ua,\ max}+l_{ua,\ min}}{2}$;
- Configuration D1: hydraulic lift cylinders fully closed ($l_{hc} = l_{hc,\ min}$; $\varphi_c = \varphi_{c,\ min}$);
- Configuration D2: hydraulic lift cylinders fully extended ($l_{hc} = l_{hc,\ max}$; $\varphi_c = \varphi_{c,\ max}$).

The kinematic analysis of the TPH in these configurations allows to determine the lower hitch point heights above the ground $H_{lad,\ min}$ and $H_{lad,\ max}$ (Figure A1d) and, ultimately, the movement range as the difference between the two.

Configurations E1 and E2 (Figure A1e,f)

These configurations are used to enforce the constraint on the mast adjustment as defined by ISO-730. The Standard sets two limit TPH configurations (by prescribing the height of the lower hitch points above the ground) and prescribes that for any configurations in between these two, the implement mast needs to range from a minimum angle of 85° with respect to the horizontal (80° for category 1N TPHs) to a maximum angle of 95° with respect to the horizontal (90° for category 1N TPHs).

From simple geometrical considerations, it emerges that the most critical configuration for meeting the requirement on the maximum mast angle is the one where the lower hitch points are the lowest, while the most critical configuration for meeting the requirement on the minimum mast angle is the other. Therefore, two configurations are set as follows:

- E1: height of lower hitch points above the ground set at the value $H_{ma,\ min}$ prescribed by the Standard (ISO-730, Table 3, No. 3.2.22 "lowest position"); upper arm set at minimum length: $l_{ua} = l_{ua,\ min}$;
- E2: height of lower hitch points above the ground set at the value $H_{ma,\ max}$ prescribed by the Standard (ISO-730, Table 3, No. 3.2.22 "highest position"); upper arm set at maximum length: $l_{ua} = l_{ua,\ max}$.

From the kinematic analysis of the TPH in configuration E1, the maximum mast angle $\varphi_{i,\ max}$ is determined and constraint C35 is enforced; the same analysis performed in configuration E2 allows to determine the minimum mast angle $\varphi_{i,\ min}$ and enforce constraint C36.

References

1. Renius, K.T. *Fundamentals of Tractor Design*; Springer Nature: Cham, Switzerland, 2020. [CrossRef]
2. Zoz, F.M.; Grisso, R.D. *Traction and Tractor Performance*; ASAE: St. Joseph, MI, USA, 2003; Volume 27.
3. Gu, Y.; Kushwaha, R.L. Dynamic Load Distribution and Tractive Performance of a Model Tractor. *J. Terramechanics* **1994**, *31*, 21–39. [CrossRef]
4. Collins, T.S. Loads in Tractor Linkages When Transporting Rear-Mounted Implements: Development of Modelling and Measurement Techniques. *J. Agric. Eng. Res.* **1991**, *49*, 165–188. [CrossRef]
5. Macmillan, R.H. *The Mechanics of Tractor-Implement Performance*; The University of Melbourne: Melbourne, Austalia, 2003.
6. Mattetti, M.; Molari, G.; Sereni, E. Damage Evaluation of Driving Events for Agricultural Tractors. *Comput. Electron. Agric.* **2017**, *135*, 328–337. [CrossRef]
7. *ASAE Standards S217.12*; Three-Point Free-Link Attachment for Hitching Implements to Agricultural Wheel Tractors. American Society of Agricultural and Biological Engineers: St. Joseph, MI, USA, 2001.
8. *ISO 730:2009*; Agricultural Wheeled Tractors—Rear-Mounted Three-Point Linkage—Categories 1N, 1, 2N, 2, 3N, 3, 4N and 4. American Society of Agricultural and Biological Engineers: St. Joseph, MI, USA, 2009; 1.
9. Morling, R.W. Agricultural tractor hitches analysis of design requirements. *ASAE Disting. Lect.* **1979**, *5*, 1–28.
10. Johansson, S. Design of a Three-Point Hitch. Master's Thesis, Linköping University, Linköping, Sweden, 2008.
11. Ambike, S.S.; Schmiedeler, J.P. Application of Geometric Constraint Programming to the Kinematic Design of Three-Point Hitches. *Appl. Eng. Agric.* **2007**, *23*, 13–21. [CrossRef]
12. Kumar, A.; Pranav, P.K.; Kumar, S. Computer Simulation of Three-Point Linkage Parameters for Virtual Hitch Point and Optimum Depth of Operation. *Eng. Agric. Environ. Food* **2018**, *11*, 114–121. [CrossRef]
13. Prasanna Kumar, G.V. Development of a Computer Program for the Path Generation of Tractor Hitch Points. *Biosyst. Eng.* **2012**, *113*, 272–283. [CrossRef]

14. Dhruw, L.K.; Pareek, C.M.; Singh, N. A Visual Basic Programme for Performance Evaluation of Three-Point Linkage Hitch System of Agricultural Tractors. *Curr. J. Appl. Sci. Technol.* **2018**, *28*, 1–12. [CrossRef]
15. Molari, G.; Mattetti, M.; Guarnieri, A. Optimal Three-Point Hitch Design to Maximize Lifting Performance. *Trans. ASABE* **2014**, *57*, 371–379.
16. OECD. *Code 2: OECD Standard Code for the Official Testing of Agricultural and Forestry Tractor Performance*; Organization for Economic Cooperation and Development: Paris, France, 2012.
17. Bauer, F.; Porteš, P.; Slimařík, D.; Čupera, J.; Fajman, M. Observation of Load Transfer from Fully Mounted Plough to Tractor Wheels by Analysis of Three Point Hitch Forces during Ploughing. *Soil Tillage Res.* **2017**, *172*, 69–78. [CrossRef]
18. Godwin, R.J.; O'Dogherty, M.J. Integrated Soil Tillage Force Prediction Models. *J. Terramechanics* **2007**, *44*, 3–14. [CrossRef]
19. Schuring, D.J.; Emori, R.I. Soil Deforming Processes and Dimensional Analysis. *SAE Trans.* **1965**, *73*, 485–494.
20. Godwin, R.J.; O'Dogherty, M.J.; Saunders, C.; Balafoutis, A.T. A Force Prediction Model for Mouldboard Ploughs Incorporating the Effects of Soil Characteristic Properties, Plough Geometric Factors and Ploughing Speed. *Biosyst. Eng.* **2007**, *97*, 117–129. [CrossRef]
21. Grisso, R.D.; Yasin, M.; Kocher, M.F. Tillage Implement Forces Operating in Silty Clay Loam. *Trans. ASAE* **1996**, *39*, 1977–1982. [CrossRef]
22. Payne, P.; Tanner, D. The Relationship between Rake Angle and the Performance of Simple Cultivation Implements. *J. Agric. Eng. Res.* **1959**, *4*, 312–325.
23. Hettiaratchi, D.R.P.; Reece, A.R. The Calculation of Passive Soil Resistance. *Geotechnique* **1974**, *24*, 289–310. [CrossRef]
24. Godwin, R.J. A Review of the Effect of Implement Geometry on Soil Failure and Implement Forces. *Soil Tillage Res.* **2007**, *97*, 331–340. [CrossRef]
25. Ibrahmi, A.; Bentaher, H.; Hbaieb, M.; Maalej, A.; Mouazen, A.M. Study the Effect of Tool Geometry and Operational Conditions on Mouldboard Plough Forces and Energy Requirement: Part 1. Finite Element Simulation. *Comput. Electron. Agric.* **2015**, *117*, 258–267. [CrossRef]
26. Ibrahmi, A.; Bentaher, H.; Hamza, E.; Maalej, A.; Mouazen, A.M. Study the Effect of Tool Geometry and Operational Conditions on Mouldboard Plough Forces and Energy Requirement: Part 2. Experimental Validation with Soil Bin Test. *Comput. Electron. Agric.* **2015**, *117*, 268–275. [CrossRef]
27. Melzi, S.; Negrini, S.; Sabbioni, E. Numerical Analysis of the Effect of Tire Characteristics, Soil Response and Suspensions Tuning on the Comfort of an Agricultural Vehicle. *J. Terramechanics* **2014**, *55*, 17–27. [CrossRef]
28. Qin, J.; Zhu, Z.; Ji, H.; Zhu, Z.; Li, Z.; Du, Y.; Song, Z.; Mao, E. Simulation of Active Steering Control for the Prevention of Tractor Dynamic Rollover on Random Road Surfaces. *Biosyst. Eng.* **2019**, *185*, 135–149. [CrossRef]
29. Zheng, E.; Cui, S.; Yang, Y.; Xue, J.; Zhu, Y.; Lin, X. Simulation of the Vibration Characteristics for Agricultural Wheeled Tractor with Implement and Front Axle Hydropneumatic Suspension. *Shock Vib.* **2019**, *2019*, 9135412. [CrossRef]
30. Zheng, E.; Zhong, X.; Zhu, R.; Xue, J.; Cui, S.; Gao, H.; Lin, X. Investigation into the Vibration Characteristics of Agricultural Wheeled Tractor-Implement System with Hydro-Pneumatic Suspension on the Front Axle. *Biosyst. Eng.* **2019**, *186*, 14–33. [CrossRef]
31. Raper, R. Force requirements and soil disruption of straight and bentleg subsoilers for conservation tillage systems. *Appl. Eng. Agric.* **2005**, *21*, 787–794. [CrossRef]